

Nanoscale

Accepted Manuscript



This is an *Accepted Manuscript*, which has been through the Royal Society of Chemistry peer review process and has been accepted for publication.

Accepted Manuscripts are published online shortly after acceptance, before technical editing, formatting and proof reading. Using this free service, authors can make their results available to the community, in citable form, before we publish the edited article. We will replace this *Accepted Manuscript* with the edited and formatted *Advance Article* as soon as it is available.

You can find more information about *Accepted Manuscripts* in the [Information for Authors](#).

Please note that technical editing may introduce minor changes to the text and/or graphics, which may alter content. The journal's standard [Terms & Conditions](#) and the [Ethical guidelines](#) still apply. In no event shall the Royal Society of Chemistry be held responsible for any errors or omissions in this *Accepted Manuscript* or any consequences arising from the use of any information it contains.

Cite this: DOI: 10.1039/c0xx00000x

www.rsc.org/xxxxxx

ARTICLE TYPE

Self-assembled 3D Pt/TiO₂ architecture for high-performance photocatalytic hydrogen production

Haiyan Li,^a Hongwen Yu,^{*a} Lei Sun,^a Jiali Zhai^a and Xuerong Han^{*b}

Received (in XXX, XXX) Xth XXXXXXXXX 20XX, Accepted Xth XXXXXXXXX 20XX

DOI: 10.1039/b000000x

3D Pt/TiO₂ architecture assembled from 1D nanowires have been designed and successfully prepared by an environmentally-friendly one-pot solvothermal process. The formation mechanism has been investigated and the unique architecture exhibits an excellent photocatalytic hydrogen production rate as high as 13.33 mmol h⁻¹g⁻¹, the corresponding apparent quantum efficiency reaches 34 %.

1. Introduction

Due to increasingly serious energy shortages and environmental crises, the development of clean and renewable energy sources has attracted great attention. Hydrogen energy is an ideal candidate and developmental planning has been successfully established in many countries.¹ Since the first discovery of photoelectrochemical splitting of water on a TiO₂ electrode in 1972 by Fujishima and Honda, photocatalytic water splitting on semiconductor photocatalysts using solar energy has been considered to be an effective and promising method for hydrogen production.² Among the various semiconductor photocatalysts investigated, TiO₂ appears to be one of the most promising photocatalysts because it is chemically inert, environmentally compatible, low in cost and displays excellent photostability.³ However, because the photoconversion efficiency of TiO₂ is limited, the rational design and preparation of TiO₂ photocatalysts with high quantum efficiency for water splitting have been the major challenges in recent years.

The quantum efficiency (QE) for hydrogen production in a powder photocatalytic system is strongly dependent on the structures of the photocatalyst and the cocatalyst. Generally, the characteristics of photocatalysts such as high crystallinity, low defect density, short charge-transfer distance, large surface area, and special morphology usually can enhance the photocatalytic performance. Thus, constructing TiO₂ nanomaterial into 3D hierarchical architectures has attracted research interest in recent years. Especially, the flowerlike hierarchical nanostructures organized from 1D nanowires are attractive photocatalyst materials in view of their higher surface-to-volume ratio and shorter transport path for minority carriers.⁴ Many methods have been developed to fabricate 3D TiO₂ architecture. The most popular process involves a template-based method, in which hard or soft templates have been used as structure-directing agents.⁵ The ability to construct complicated structures has been limited by the availability of suitable templates. Moreover, the removal of

the template requires either harsh chemical reactions or high temperature calcinations which must be finely controlled to avoid structure collapse. As an alternative, template-free approaches based on different mechanisms have also been developed, but these techniques often need microwave irradiation, or reagents such as H₂O₂, benzene, toluene, or ethylenediamine,⁶ etc. These agents are either toxic or hazardous and pose environmental and health risks. Thus, the development of a template-free, environmentally-friendly preparative strategy would be significant and highly desired.

To date, hydrogen production using a TiO₂ photocatalyst has mainly relied on the Pt or Pt-based cocatalysts due to their negligible overpotential and excellent kinetics for the hydrogen production reaction.⁷ Loading of Pt nanoparticles onto the TiO₂ surface has been proven to show greater efficiency for photocatalytic water splitting in the presence of sacrificial reagents. Presently, loading of the Pt cocatalyst onto the TiO₂ photocatalyst surface is usually achieved by photodeposition and impregnation-calcination methods, which require a light source, a sacrificial reagent, or high-temperature calcining treatment, and thus, the process is relatively complicated.⁸ In light of the above problems, we undertook the development of a one-pot green synthesis procedure to prepare a 3D Pt/TiO₂ architecture organized from 1D nanowires. We proposed to prepare a photocatalytic system with the advantages of a high aspect ratio, shorter diffusion distance for minority carriers, and larger specific surface area which would be uniquely suited for photocatalytic H₂ production. Indeed, we expected that the new 3D Pt/TiO₂ architecture could exhibit a remarkable increase in photocatalytic activity.

In this communication, we report for the first time the fabrication of a 3D Pt/TiO₂ architecture assembled from 1D nanowires by a simple one-pot solvothermal method using Ti(OC₄H₉)₄ and H₂PtCl₆ as precursors, ethylene glycol (EG) as the chelating and reducing agent. The 3D architecture with a size of about 2-3 μm was high in anatase crystallinity, and the Pt nanoparticles were uniformly dispersed throughout the whole architecture. The morphology evolution and formation mechanism of the Pt/TiO₂ architecture were investigated, and the EG and H₂PtCl₆ were found to play critical roles in controlling the morphology of Pt/TiO₂ architecture. The as-prepared Pt/TiO₂ architecture displayed unique characteristic, including large specific surface area, enhanced light harvesting, short charge-transfer distance, and excellent charge transfer. This material

exhibited outstanding photocatalytic hydrogen production activity, and the apparent QE was as great as 34 % at 365 nm wavelength.

2. Experimental section

2.1. Synthesis of 3D Pt/TiO₂ architecture

3D Pt/TiO₂ architecture was prepared by a one-pot solvothermal method. All the chemicals were of analytical grade and were used as received without further purification. Distilled water was used in all experiments. In a typical synthesis, solutions of tetrabutyl titanate (Ti(OC₄H₉)₄, 0.2 M in ethylene glycol), chloroplatinic acid (H₂PtCl₆, 4.6 mM in ethylene glycol), and sodium hydroxide (NaOH, 10 M in water) were prepared as stock solutions in advance. A certain amount of H₂PtCl₆ stock solution was mixed with 10 mL of tetrabutyl titanate stock solution under vigorous stirring, then, the above mixed solution was added into 10 mL of NaOH aqueous solution. After that, the system was sealed with Parafilm (Pechiney Plastic Packaging, Inc., Chicago, IL) and was kept stirring for 1 h. then transferred into a Teflon-lined stainless steel autoclave (50 mL) and heated at 200 °C for 16 h. The resulting light gray precipitate was harvested by centrifugation, followed by washing with 0.2 M HCl, deionized water and ethanol until the pH value of the washings was about 7 and remove residual EG on the surface. After the washing treatment, the sample was dried under vacuum overnight and sequentially calcined in a muffle furnace at 500 °C for 2 h. The pure sample of TiO₂ nanowires was prepared without adding H₂PtCl₆ in the above method.

2.2. Characterizations

Crystalline phases were examined by X-ray diffraction (XRD) using a Rigaku D/Max-2550 diffractometer with Cu_{Kα} radiation ($\lambda = 1.54056 \text{ \AA}$) at 50 kV and 200 mA in the 2 θ range 20–80° with a scanning rate of 5° min⁻¹. Scanning electron microscopy (SEM) measurements were made by using a XL30 ESEM FEG scanning electron microscope (FEI Company). Transmission electron microscopy (TEM) measurements were made by using a HITACHI H-8100 EM (Hitachi, Tokyo, Japan). The Brunauer–Emmett–Teller (BET) surface areas and porosity of the samples were determined using a Micro-meritics ASAP 2020 nitrogen adsorption apparatus. All the samples were degassed at 180 °C prior to nitrogen adsorption measurements. The BET surface area was determined by a multipoint BET method using adsorption data in the relative pressure (P/P_0) range of 0.05–0.3. Desorption data were used to determine the pore size distribution via the Barret-Joyner-Halender (BJH) method. The volume of adsorbed nitrogen at the relative pressure (P/P_0) of 0.969 was used to determine the pore volume and average pore size. The loading contents of Pt for all samples were measured by Inductively Coupled Plasma optical emission spectrometer (ICP-OES, Focused Photonics).

2.3. Photoelectrochemical measurements

Photoelectrochemical measurements were composed of a CHI 660D electrochemical analyzer (CH Instruments, Inc., Shanghai), a 500 W xenon lamp (CHFXQ500W, Beijing) with a band-pass filter ($\lambda = 365 \text{ nm}$), and a homemade three-electrode cell using a KCl-saturated Ag/AgCl electrode, a platinum wire, and Pt/TiO₂ sample as the reference, counter, and working electrodes,

respectively. Pt/TiO₂ electrodes were prepared by depositing suspensions made of Pt/TiO₂ and absolute ethanol onto Indium-Tin Oxide glass (ITO). The supporting electrolyte was 1 M Na₂SO₄ aqueous solution, which was purged with high-purity nitrogen for at least 15 min prior to experiments.

2.4. Photocatalytic H₂ evolution

The photocatalytic reaction was carried out in a Pyrex reaction cell connected to a closed gas circulation and evacuation system (Fig. S1). A 300 W Xe lamp equipped with a 365 nm band-pass filter was used as light source, and the focused intensity on the flask was ca. 20 mW/cm². In a typical photocatalytic experiment, 50 mg of the as-prepared Pt/TiO₂ architecture sample was dispersed in 50 mL aqueous solution containing 10 ml of 20 vol % CH₃OH as a sacrificing agent. Before irradiation, the suspension was dispersed by ultrasonic and bubbled with nitrogen to remove the dissolved oxygen. The H₂ gas evolution was measured by on-line gas chromatography (CLARUS 580 GC, PerkinElmer) with thermal conductivity detector and nitrogen carrier gas. The comparison experiments were prepared with the same quality of the photocatalysts. The apparent QE was measured under the same photocatalytic reaction conditions and it was calculated according to the following equation:

$$\begin{aligned} \text{QE} [\%] &= \frac{\text{number of reacted electrons}}{\text{number of incident electrons}} \times 100 \\ &= \frac{\text{number of evolved H}_2 \text{ molecules} \times 2}{\text{number of incident photons}} \times 100 \end{aligned} \quad (\text{i})$$

The number of incident photons was 6.61×10^{17} photons/s which was measured by using a calibrated Si photodiode.

3. Results and discussion

The structures of the as-prepared architecture were first characterized by scanning electron microscopy (SEM) and transmission electron microscopy (TEM), as shown in Fig. 1. The as-prepared products displayed a 3D hierarchical structure of 2–3 μm (Fig. 1a, c). A magnified image confirmed that the hierarchical structure consisted of self-supported radial 1D nanowires with a large surface area and a high surface-to-volume ratio (Fig. 1b). TEM images showed the as-prepared samples to be nearly spherical in morphology, with sea-urchin-like structures (Fig. 1c). Especially, the gradual contrast of the TEM image from the edge to the center of the sphere indicated that the entire sphere was composed of self-organized 1D nanowires. The HRTEM image taken from a single nanowire (inset in Fig. 1c) indicated the nanowire consisted of highly crystallized anatase with a crystalline lattice of 0.35 nm, corresponding to the (101) crystallographic plane of TiO₂.⁹ The high magnification TEM image shown in Fig. 1d indicated that a large amount of nanoparticles were generated on the surface of TiO₂ nanowires, and the HRTEM image taken from one nanoparticle revealed clear lattice fringes with an inter-plane distance of 0.23 nm, corresponding to the (111) lattice plane of face-centered cubic (fcc) Pt (Fig. 1e). Moreover, with increasing the initial Pt content, the corresponding amounts of Pt nanoparticles on the surface of TiO₂ nanowires increased, as shown in Fig. S2. The EDS mapping images further confirmed the sample contains Ti, O, and Pt elements (Fig. 1f). The sparse and uniform distribution of Pt

nanoparticles throughout the whole architecture was clearly observed. The crystalline nature of the Pt/TiO₂ architecture was further examined by XRD analysis (Fig. S3). All the samples clearly exhibited similar XRD patterns that could be indexed to anatase (JCPDS file No. 21-1272). However, no obvious diffraction peaks of Pt phase were observed, which may be attributed to the very low concentration of Pt added in the sample, making them barely measurable.

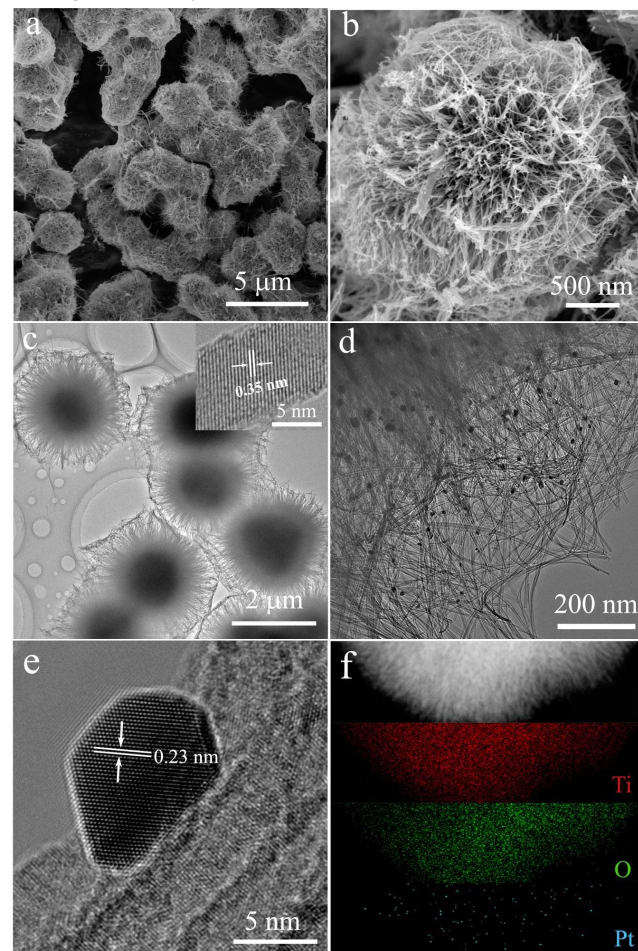


Fig. 1 (a) Typical SEM, (b) magnified SEM, (c, d) TEM and (e) HRTEM images of the as-prepared 0.4 wt % Pt/TiO₂ architecture (inset: HRTEM micrograph with the lattice fringes). (f) EDS mapping of Ti, O and Pt elements.

The N₂ adsorption-desorption isotherms measured on the Pt/TiO₂ architecture show hysteresis loops at relative pressures close to unity (Fig. S4), indicating the presence of large mesopores and macropores, which categorize them as type IV according to IUPAC classification.¹⁰ The pore-size distributions (inset in Fig. S2) indicated that the Pt/TiO₂ architecture exhibited wide pore-size distributions ranging from 2 to 100 nm. Table S1 lists the Brunauer-Emmett-Teller (BET) surface areas, average pore sizes and pore volumes of the different samples. As measured, the 0.4 wt % Pt/TiO₂ architecture enhanced the BET surface areas (87.1 m²/g) greatly in contrast to that of pure TiO₂ nanowires (12.2 m²/g). Such organized porous structures might be extremely useful in photocatalysis because they possess efficient transport pathways for reactant and product molecules.

To elucidate the growth process of the 3D Pt/TiO₂ architecture, we followed the growth steps of the samples at different reaction

stages by SEM, as shown in Fig. 2. At a short reaction time of 35 min, the sample displayed slightly aggregated sphere morphology with an average size of ~500 nm. The entire hierarchical sphere was composed of self-organized TiO₂ nanosheets with random orientations (Fig. 2a, b). When the reaction time was prolonged to 50 min, the samples kept the spherical morphologies, but the average size increased to ~1.5 μm. Furthermore, we propose that the above nanosheets were not stable under the present reaction conditions and they tended to curl into nanotubes, which would account for the obvious hollow tubular structures (Fig. 2c, d). When the reaction time was extended to 60 min, the assembled sphere grew further, and the average size reached ~2 μm. Notably, the hollow tubular structures disappeared, and instead, numerous nanowires were generated (Fig. 2e, f). After the reaction time for 5 h, well-organized 3D hierarchical spheres with the size of 2-3 μm were formed and the morphology showed less change even if the reaction time was further increased (Fig. S5). These experimental results indicated that the 3D Pt/TiO₂ architecture was achieved in three stages: nanosheet-nanotube-nanowire.

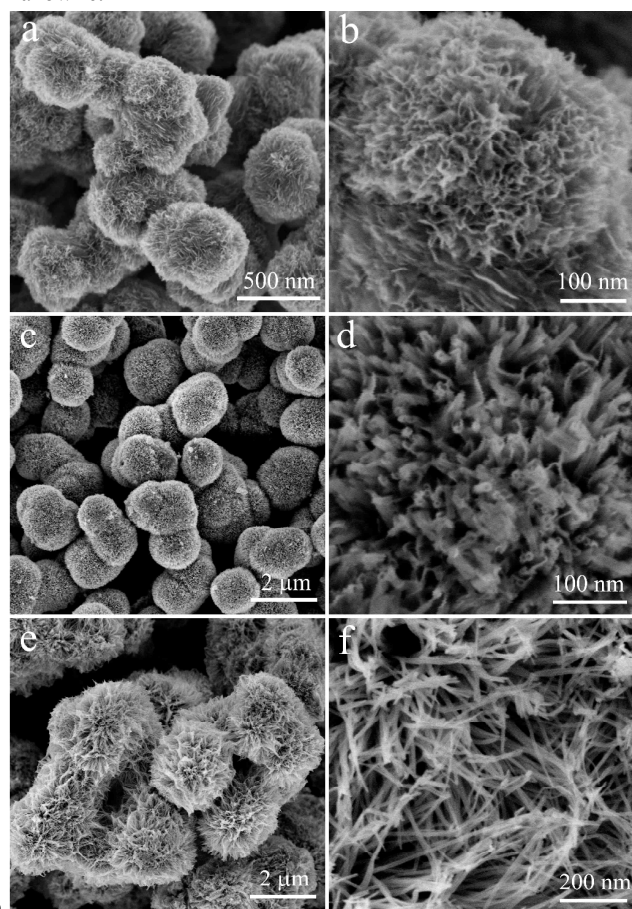


Fig. 2 SEM images of the 0.4 wt % Pt/TiO₂ architecture obtained with different reaction times. (a, b) 35 min; (c, d) 50 min; (e, f) 60 min.

To examine the effects of EG and H₂PtCl₆ in the synthesis of TiO₂ architecture, we performed a series of comparative experiments to explore the formation process. When the ethanol (ET) was used as solvent instead of EG (Fig. S6a), the 3D architecture was not formed, but instead many nanowires were obtained and Pt nanoparticles on the nanowire surfaces were clearly visible. Similarly, many nanowires of several micrometers

were obtained without the addition of H_2PtCl_6 into the system, as shown in Fig. S6b. These results indicate that the EG and H_2PtCl_6 play a critical role in the synthesis of 3D Pt/TiO₂ architecture. During the solvothermal process, we assumed that a TiO₂ cluster or crystal nucleus was formed in solution phase by the slow hydrolysis of Ti precursor, the nucleus was then agglomerated and grew into nanosheets.¹¹ At the same time, the EG served as a reducing agent, the Pt crystal nucleus was formed.¹² The presence of Pt nucleus as seeds prompted the self-assembly of TiO₂ nanosheets, then, gradually forming 3D spheres. Under elevated temperature conditions, these nanosheets tended to curl into nanotubes, and ultimately, transformed into nanowires, because sufficient energy was provided to overcome the strain energy barrier, which was consistent with the rolling growth mechanism previously reported.¹³

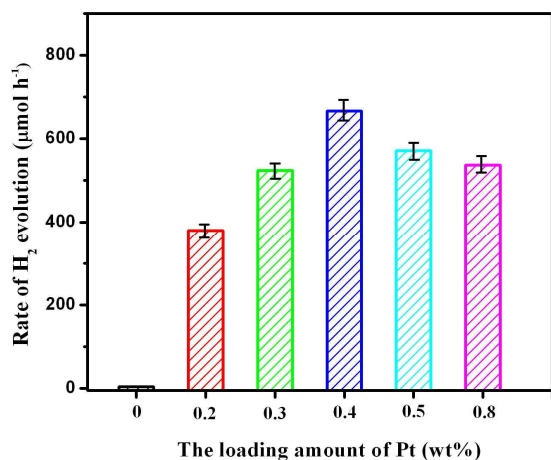


Fig. 3 The rate of H₂ evolution by Pt/TiO₂ photocatalysts loaded with different amounts of Pt. Reaction conditions: catalyst, 50 mg; 20 vol % CH₃OH solution, 50 ml; light source, 300 W Xe lamp with a 365 nm filter.

To examine the photocatalytic behavior of the 3D Pt/TiO₂ architecture, we performed photocatalytic H₂ evolution experiments with CH₃OH as the sacrificial agent. A series of 3D Pt/TiO₂ photocatalysts with different amounts of Pt was prepared, and the loading contents of Pt for all samples were measured by ICP-OES. For sample 0.2 wt % Pt/TiO₂, the Pt content measured was 0.19 wt%, which is close to the initial one. With increasing the initial Pt content, the corresponding measured Pt increased, which is 0.28, 0.36, 0.41 and 0.61 wt% for 0.3, 0.4, 0.5 and 0.8 wt% Pt/TiO₂ samples (Table S1). Control experiments indicated that no appreciable hydrogen production was detected in the absence of either irradiation or photocatalyst, suggesting that hydrogen was produced via the photocatalytic reactions. Fig. 3 compares the photocatalytic H₂ evolution activity of pristine TiO₂ nanowire and Pt/TiO₂ architecture loaded with different amounts of Pt. Pure TiO₂ nanowire showed negligible H₂ evolution activity because of the rapid recombination of the conduction band electrons and the valence band holes and the presence of a large overpotential in the production of H₂. However, the 3D Pt/TiO₂ architecture showed highly efficient photocatalytic activity, and the photocatalytic activity of the as-prepared samples increased as the Pt content increased from 0.2 to 0.4 wt %, the rate of H₂ evolution is about 380, 524, 667 μmol h⁻¹ for 0.2, 0.3, and 0.4 wt % Pt/TiO₂ architecture, respectively. The highest H₂-evolution rate, obtained for the 0.4 wt % Pt/TiO₂

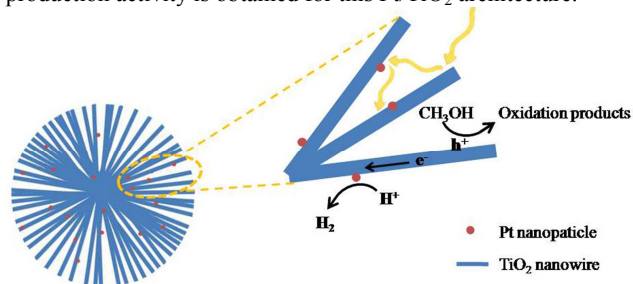
sample, was 667 μmol h⁻¹, corresponding to an apparent QE of 34 % at 365 nm. This value exceeded that obtained with pure TiO₂ nanowire (3.7 μmol h⁻¹) and 0.4 wt % Pt/P25 (220 μmol h⁻¹, Fig. S7) by factors of 180 and 3, respectively. To our best knowledge, this value of QE exceeded the results obtained with some TiO₂-based photocatalysts reported so far.¹⁴ The excellent photocatalytic activity of Pt/TiO₂ architecture was recorded by video, and plentiful bubbles were observed clearly upon irradiation (Movie S1). When the Pt content was increased over 0.4 wt %, the photocatalytic activity was gradually reduced, which can be attributed to the excessive Pt on the TiO₂ surface will increase the opacity and light scattering of the suspension solution, thereby reducing the photon absorption of TiO₂. Moreover, Pt as cocatalyst at high content may act as charge recombination centers, resulting in the decrease of the photocatalytic activity.¹⁵ This relationship suggests that a good dispersion of the optimal amount of Pt is necessary.¹⁶

In addition to high photocatalytic activity, a high performance photocatalyst must display good stability. The time courses of photocatalytic hydrogen evolution for the 0.4 wt % Pt/TiO₂ were recorded to evaluate its stability (Fig. S8). Remarkably, no loss in catalytic activity was observed in the recycling reactions demonstrating the good stability of the Pt/TiO₂ architecture. Thus, all above-mentioned results indicate that the hierarchical Pt/TiO₂ architecture is a promising candidate for photocatalysts.

Transient photocurrent measurements were performed to evaluate the charge carrier properties of the 0.4 wt % Pt/TiO₂ architecture, as shown in Fig. S9. To compare the photocurrent response, the pure 0.4 wt % Pt/TiO₂ nanowires were also examined. We observed an anodic photocurrent, which is characteristic of n-type semiconductors. However, the Pt/TiO₂ architecture exhibited a noticeable improvement of the photocurrent value with respect to the Pt/TiO₂ nanowires, while the enhanced photocurrent response of Pt/TiO₂ architecture indicated a higher separation efficiency of the photoinduced electron-hole pairs and a lower recombination rate in such structures.¹⁷ It is worth noting that the photocurrent of Pt/TiO₂ architecture rapidly reached a maximum and then rapidly returned to the initial value as the light is switched on and off, indicating the excellent ability of photoelectric conversion. The improved charge separation should be attributed to the structural benefits of the Pt/TiO₂ architecture, since the 1D nanowires with higher surface-to-volume ratio can significantly shorten the diffusion distance of charge and inhibit the electron-hole recombination, which is favorable for the improvement of photocatalytic performance.

Based on the above results, we propose a tentative mechanism for the high H₂ production activity of the 3D Pt/TiO₂ photocatalysts (Scheme 1). First, the unique architecture of Pt/TiO₂ favors the multiple light absorbance and reflections within the chamber, enhancing the light harvesting.¹⁸ Under irradiation by UV light, the TiO₂ is excited, the electrons are transferred from valence band to conduction band, and subsequently are easily transferred to the Pt nanoparticles. Because the Fermi level of Pt (E_F=0.66 V vs. NHE) is lower than that of the TiO₂ semiconductor (E_F=-0.21 V vs. NHE), the excited electrons on the conduction band of TiO₂ could overcome the Schottky barrier and are readily transferred to the Fermi level of Pt.¹⁹ Then, the Pt

nanoparticles as the cocatalyst can promote the separation of photo-induced electrons and effectively reduce H^+ to produce H_2 molecules. Moreover, the 3D architecture assembled from nanowires with a high aspect ratio can shorten the minority charge carrier transport distance to the electrolyte, thus, allowing the photo-induced hole to quickly diffuse to the surface of the nanowires, and react with the methanol solution to generate the oxidation products. This process can accelerate the separation of photo-induced electron-hole pairs, and inhibit their recombination. Therefore, it is not surprising that a highly efficient H_2 -production activity is obtained for this Pt/TiO₂ architecture.



Scheme 1 Schematic representation of the charge transfer in 3D Pt/TiO₂ photocatalysts.

4. Conclusions

In conclusion, for the first time, a 3D Pt/TiO₂ architecture has been prepared via a simple, environmentally-friendly, one-pot solvothermal method without adding any template. This 3D structure with a size of about 2-3 μm consists of many 1D TiO₂ nanowires with random orientations, with the Pt nanoparticles uniformly dispersed throughout the whole architecture. The evolution of the morphology and the formation mechanism of the 3D Pt/TiO₂ architecture confirmed that the EG and H_2PtCl_6 play critical roles in controlling the morphology of the Pt/TiO₂ architecture. The Pt/TiO₂ architecture showed an excellent photocatalytic hydrogen production activity, with a maximum hydrogen production rate of 13.33 $\text{mmol h}^{-1}\text{g}^{-1}$ at Pt loading content of 0.4 wt %; the corresponding apparent QE reached 34 % at 365 nm. This excellent photocatalytic activity is ascribed to the combined effects of the following three factors: (1) The architecture permits excellent depth of light absorption; (2) The larger specific surface area provided more surface active sites for photocatalytic reaction; (3) 1D nanowires with a high aspect ratio can shorten the transport distance between the minority and the electrolyte, enhancing the separation of photoinduced electron-hole pairs and inhibiting their recombination. Such 3D Pt/TiO₂ architecture is promising as a universal and effective photocatalyst for photocatalytic hydrogen production.

Acknowledgements

This work was supported by the National Natural Science Foundation of China (No. 2177142), the Important Deployment Project of Chinese Academy of Sciences (KZZD-EW-TZ-16), the Excellent Young Scientists Foundation of the Northeast Institute of Geography and Agroecology (DLSYQ14001) and the Project of Science and Technology Development Plan of Jilin Province (No. 20140520092JH).

Notes and references

- ^a Key Laboratory of Wetland Ecology and Environment, Northeast Institute of Geography and Agroecology, Chinese Academy of Sciences, Changchun 130102, China. Tel: (+86)-431-85542290; E-mail: yuhw@neigae.ac.cn;
- ^b Faculty of Advanced Life Science, Hokkaido University, Sapporo 001-0021, Japan. E-mail: hxr@mail.sci.hokudai.ac.jp
- † Electronic Supplementary Information (ESI) available: Characterization data of photocatalysts, and a movie in avi format are available. See DOI: 10.1039/b000000x/
- 1 Y. Q. Wu, G. X. Lu and S. B. Li, *J. Phys. Chem. C*, 2009, **113**, 9950.
 - 2 A. Fujishima and K. Honda, *Nature*, 1972, **238**, 37; Y. Zhong, K. Ueno, Y. Mori, X. Shi, T. Oshikiri, K. Murakoshi, H. Inoue and H. Misawa, *Angew. Chem. Int. Ed.*, 2014, **53**, 10350.
 - 3 Asahi, R. Morikawa, T. Ohwaki, T. Aoki and K. Y. Taga, *Science*, 2001, **293**, 269; G. Liu, L. C. Yin, J. Q. Wang, P. Niu, C. Zhen, Y. P. Xie and H. M. Cheng, *Energy Environ. Sci.*, 2012, **5**, 9603; A. Kudo and Y. Miseki, *Chem. Soc. Rev.*, 2009, **38**, 253; Y. Nishijima, K. Ueno, Y. Kotake, K. Murakoshi, H. Inoue and H. Misawa, *J. Phys. Chem. Lett.*, 2012 **3**, 1248.
 - 4 F. E. Osterloh, *Chem. Soc. Rev.*, 2013, **42**, 2294; S. Hoang, S. P. Berglund, N. T. Hahn, A. J. Bard and C. B. Mullins, *J. Am. Chem. Soc.*, 2012, **134**, 3659; J. H. Park, S. Kim and A. J. Bard, *Nano Lett.*, 2006, **6**, 24.
 - 5 J. Q. Huang, Z. Huang, W. Guo, M. L. Wang, Y. G. Cao and M. C. Hong, *Cryst. Growth Des.*, 2008, **8**, 2444. M. C. Lechmann, D. Kessler and J. S. Gutmann, *Langmuir*, 2009, **25**, 10202.
 - 6 D. Zhang, G. Li, F. Wang and J. C. Yu, *CrystEngComm*, 2010, **12**, 1759; C. Wang, L. Yin, L. Zhang, Y. Qi, N. Lun and N. Liu, *Langmuir*, 2010, **26**, 12841; X. Li, Y. Xiong, Z. Li and Y. Xie, *Inorg. Chem.*, 2006, **45**, 3493; S. Yang and L. Gao, *Mater. Chem. Phys.*, 2006, **99**, 437; L. Q. Xiang, X. P. Zhao, J. B. Yin and B. L. Fan, *J. Mater. Sci.*, 2012, **47**, 1436; T. J. Zhu, J. Li and Q. S. Wu, *ACS Appl. Mater. Interfaces*, 2011, **3**, 3448.
 - 7 X. Zong, H. J. Yan, G. P. Wu, G. J. Ma, F. Y. Wen, L. Wang and C. Li, *J. Am. Chem. Soc.*, 2008, **130**, 7176; H. Kato and A. Kudo, *J. Phys. Chem. B*, 2001, **105**, 4285; K. Maeda, T. Saito, T. Takata, N. Saito, Y. Inoue and K. J. Domen, *Phys. Chem. B*, 2006, **110**, 4500.
 - 8 A. Galińska and J. Walendziewski, *Energy & Fuels*, 2005, **19**, 1143; J. G. Yu, L. F. Qi and M. Jaroniec, *J. Phys. Chem. C*, 2010, **114**, 13118.
 - 9 S. W. Liu, J. G. Yu and M. Jaroniec, *J. Am. Chem. Soc.*, 2010, **132**, 11914.
 - 10 K. S. W. Sing, D. H. Everett, R. A. W. Haul, L. Moscou, R. A. Pierotti, J. Rouquerol and T. Siemieniowska, *Pure Appl. Chem.*, 1985, **57**, 603; M. Kruk and M. Jaroniec, *Chem. Mater.*, 2001, **13**, 3169.
 - 11 B. M. Wen, C. Y. Liu and Y. Liu, *New J. Chem.*, 2005, **29**, 969.
 - 12 J. Y. Chen, T. Herricks, M. Geissler and Y. N. Xia, *J. Am. Chem. Soc.*, 2004, **126**, 10854.
 - 13 Y. B. Mao, M. Kanungo, T. Hemraj-Benny and S. S. Wong, *J. Phys. Chem. B*, 2006, **110**, 702; D. S. Wang, C. H. Hao, W. Zheng, X. L. Ma, D. R. Chu, Q. Peng and Y. D. Li, *Nano Res.*, 2009, **2**, 130.
 - 14 X. B. Chen, S. H. Shen, L. J. Guo, S. S. Mao, *Chem. Rev.*, 2010, **110**, 6503.
 - 15 J. Zhang, J. G. Yu, Y. M. Zhang, Q. Li and J. R. Gong, *Nano Lett.*, 2011, **11**, 4774.
 - 16 S. S. K. Ma, K. Maeda, R. Abe and K. Domen, *Energy Environ. Sci.*, 2012, **5**, 8390.
 - 17 Q. P. Luo, X. Y. Yu, B. X. Lei, H. Y. Chen, D. B. Kuang and C. Y. Su, *J. Phys. Chem. C*, 2012, **116**, 8111; X. H. Gao, H. B. Wu, L. X. Zheng, Y. J. Zhong, Y. Hu and X. W. Lou, *Angew. Chem. Int. Ed.*, 2014, **53**, 5917; I. S. Cho, Z. B. Chen, A. J. Forman, D. R. Kim, P. M. Rao, R. F. Jaramillo and X. L. Zheng, *Nano Lett.*, 2011, **11**, 4978.
 - 18 Z. Wang, J. G. Hou, C. Yang, S. Q. Jiao, K. Huang and H. M. Zhu, *Energy Environ. Sci.*, 2013, **6**, 2134.
 - 19 V. Subramanian, E. Wolf and P. V. Kamat, *J. Phys. Chem. B*, 2001, **105**, 11439; M. Anpo and M. Takeuchi, *J. Catal.*, 2003, **216**, 505; H. S. Wu, L. D. Sun, H. P. Zhou and C. H. Yan, *Nanoscale*, 2012, **4**, 3242.